ELSEVIER

Chemical Physics 213 (1996) 385–396

Chemical Physics

Photodissociation dynamics of $HN_3(DN_3) + h\nu \rightarrow H(D) + N_3$

Michael Lock, Karl-Heinz Gericke *, Franz Josef Comes

Institut für Physikalische und Theoretische Chemie, Johann Wolfgang Goethe Universität, Marie Curie Strasse 11, D-60439 Frankfurt / Main, Germany

Received 29 April 1996

Abstract

The photolysis of HN_3/DN_3 to give H/D and N_3 is investigated at different photolysis wavelengths: 266, 248, 222, 193 and 122 nm. Nascent H/D atoms are characterized via Doppler and polarization spectroscopy using laser-induced fluorescence in the VUV. The following quantum yields have been found: $\phi_{H-N_3}(266\ nm) = 0.04$, $\phi_{H-N_3}(248\ nm) \approx \phi_{D-N_3}(248\ nm) = 0.20$, and $\phi_{H-N_3}(193\ nm) \approx \phi_{D-N_3}(193\ nm) = 0.14$. At a photolysis wavelength of 266 nm most of the available energy goes into product translation, $\langle E_{kin} \rangle = 5820\ cm^{-1}$, while the internal energy of the N_3 fragment is fairly low, $\langle E_{int}(N_3) \rangle = 1250\ cm^{-1}$. At 248 nm the values are 6640 and 3150 cm^{-1}, respectively. Thus additional excess energy is preferentially released as internal energy of the N_3 radical. This trend is less pronounced when the excitation wavelength is set to 222 or 193 nm. At 122 nm the kinetic energy of the photofragments is smaller than in the 193 nm experiment. At 266 and 248 nm the spatial distribution of the photofragments is described by a strongly negative anisotropy parameter indicating a definite preference for a perpendicular alignment of the electronic transition moment and the recoil velocity vector. At 222 and 193 nm the anisotropy parameter is close to zero, while the VUV photolysis results in a slightly positive anisotropy parameter. These experimental findings indicate that the access to different electronic states of HN_3/DN_3 is gained as the photolysis wavelength is varied from 266 to 122 nm.

1. Introduction

The photodissociation of hydrazoic acid and its deuterated analogue has been object of extensive investigations. Until recently only N_2 fragments in the ground electronic state [1] and NH/ND fragments in several electronic states [2] have been detected, although the photolysis wavelength was varied over a wide range including IR [3], VIS [4–6], UV [1,2,7–15], and VUV [16,17] radiation. Only a few references gave indirect hints of another fragmentation channel leading to H/D and N_3 fragments [18–21].

In a preceding study [22], we have reported the observation of hydrogen atoms as the primary products of the one-photon dissociation of HN_3 at a photolysis wavelength of 248 and 193 nm. The quantum yield of the new fragmentation channel ϕ_{H-N_3} was determined using the photolysis of H_2S as a reference system. Only a rough estimation of the kinetic energy was given, because the analysis of the detected Doppler profiles proved to be cumbersome. It seemed that the recoil velocity distribution of the H atoms is very broad indicating a strongly excited N_3 partner fragment.

Therefore, in a second study [23], the N_3 excitation was further classified. Because several thousand rovibronic levels of the generated N_3 radicals may be

* Corresponding author. Fax: +69 798 29445.

PII S0301-0104(96)00239-X

populated [24], and the first excited state of N_3 used for LIF detection is predissociative [25], laser-induced fluorescence (LIF) is not a convenient tool for characterizing nascent N_3 products. It is more convenient to monitor the recoil velocity distribution of the H atoms by resonance-enhanced multiphoton ionization (REMPI) and time-of-flight (TOF) techniques. Through conservation of momentum and energy the H atom recoil velocity distribution reveals the distribution among the rovibronic states of the N_3 radical.

In a one-color experiment jet-cooled hydrazoic acid is dissociated by a first photon of 243 nm wavelength and the generated H fragments are ionized according to the (2 + 1) REMPI detection scheme. The obtained time-of-flight spectrum is nearly Gaussian-shaped, but small modulations are noticeable. From these modulations it is possible to derive that the symmetric stretching mode of the N_3 fragment is strongly excited [23].

The present study is directed towards characterizing the influence of different electronic states on the dissociation process. We employ five different photolysis wavelengths: 266, 248, 222, 193 and 122 nm to excite the HN_3/DN_3 molecules. In addition to the results in Refs. [22,23], the H and D atom quantum yield of HN_3 at 266 nm and of DN_3 at 248 and 193 nm are presented. Furthermore at all wavelengths are not only the recoil velocity, but also the spatial distribution of the H fragments determined using laser-induced fluorescence combined with polarization and sub-Doppler spectroscopy. Combining our experimental findings with results from absorption spectroscopy [26,27] and ab initio calculations [28–30] allows us to obtain insight into the nature of the electronic states accessed through photoexcitation at the different photolysis wavelengths as well as unravel the dynamics of the dissociation process.

2. Experimental

$HN_3(DN_3)$ is generated by dropwise addition of (deuterated) phosphoric acid to NaN_3 under vacuum. The gas is stored in a glass bulb at a maximum pressure of 10 kPa. From there $HN_3(DN_3)$ flows continuously into the observation cell. In the cell, typical pressures are in the range of 0.5 to 3 Pa. The experiments are performed with a standard laser photolysis, laser-induced fluorescence pump–probe technique. An excimer laser (Lambda Physik, EMG 201 or EMG 101) with KrF, KrCl, or ArF as active medium supplies the photolysis light of 248, 222 or 193 nm wavelength. The output of the excimer laser is passed through a Rochon polarizer. The photolysis at wavelengths of 266 and 122 nm is performed with the forth harmonic of a Nd: YAG laser (Quanta Ray, DCR 1A) or solely with the VUV probe laser. At 248 and 193 nm the pulse energy inside the cell is approximately 0.5 to 1 mJ at a beam diameter of ~ 0.3 cm. The pulse energy at 266 nm is higher and at 222 and 122 nm it is smaller.

The H/D atoms are detected by excitation of the $^2P \leftarrow {}^2S$ transition and observation of the VUV fluorescence. The tunable radiation around 122 nm is generated by frequency tripling the output of a dye laser (Lambda Physik, FL 2002 E) which is pumped by a XeCl excimer laser (Lambda Physik, LPX 100) [31–33]. The dye laser beam is focused via a quartz lens ($f = 10$ cm) into a 13 cm long cell filled with 9 kPa Kr. A LiF lens with a focal length of ~ 6.6 cm (at 122 nm) collimates the generated Lyman-α radiation. The bandwidth of the third harmonic is estimated at $\Delta\nu_{VUV} = 1.25\ cm^{-1}$ by taking spectra of thermal D atoms. Thermal D atoms are generated by the photolysis of D_2S using high inert gas pressures (up to 1 kPa He) and long delay times (up to 100 μs). The observed line profiles are deconvoluted with the contribution due to room temperature Doppler broadening ($\Delta\nu_D(300\ K) = 0.72\ cm^{-1}$) in order to obtain the bandwidth $\Delta\nu_{VUV}$ of the probe laser. The pulse energy is ~ 25 nJ ($\sim 1.5 \times 10^{10}$ photons) and the beam diameter is slightly less than 0.1 cm ensuring minor influences of saturation effects.

The VUV fluorescence is observed by a solar-blind multiplier (EMR 542G-08-18). The signal from the multiplier tube is sent to a boxcar integrator (Stanford, SRS 250) and subsequently digitized for storage and analysis in a laboratory computer (Siemens PCAT 386/7). Scattered light is reduced by a series of baffles arranged in the path of both laser beams. The influence of scattered light is further minimized by the solar-blind multiplier, gating the boxcar, and a baffle fixed between the multiplier and the crossing point of the laser beams. For determining the vector correlation the polarization plane of

the photolysis laser is rotated either parallel (geometry V, as defined in Ref. [34]) or perpendicular (geometry II) to the probe laser axis. The timing of the laser pulses is controlled by a home-built trigger device operating at a repetition rate of 10 Hz with the delay between pump and probe laser set to 50 ns.

3. Results

The H and D atom quantum yield of HN_3 at 266 nm and of DN_3 at 248 and 193 nm is measured as discussed in detail in our preceding study [22]. In short, the integrated line intensity of the D atoms generated in the DN_3 photolysis is normalized to that of the D_2S photolysis, whose quantum yield is assumed to be unity. This procedure eliminates the determination of critical quantities like absolute intensities of the pump and probe laser. The absorption cross section data, however, must be known accurately. Since no values for the absorption cross section of DN_3 and D_2S ($\lambda \geq 240$ nm) are available, we have determined these values in a separate experiment. Table 1 summarizes the quantum yields of the $H + N_3$ and $D + N_3$ channel along with the absorption cross sections used for calculation.

At an excitation wavelength of 266 nm the quantum yield of the $H + N_3$ channel amounts for only $\sim 4\%$, i.e. most of the HN_3 molecules decay into the well-known NH and N_2 products. At 248 nm, however, an essential part of the parent molecules generates H or D atoms. One might expect this increase because the energy for breaking a N–H bond is greater than for a N–N bond. But if the photolysis wavelength is set to 193 nm, the H/D atom quantum yield becomes smaller again. Within our error limits the quantum yield for H and D atom generation is the same, i.e. no isotopic effects are observable.

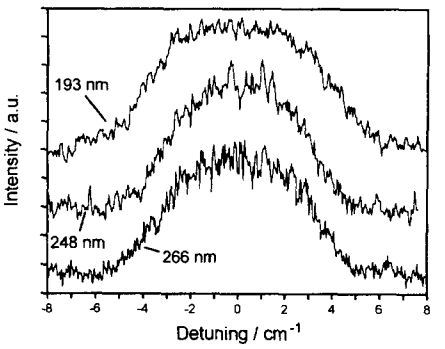

Fig. 1. H atom Doppler profiles detected after the dissociation of HN_3 at 266, 248 and 193 nm. The photolysis light is unpolarized in order to reduce the influence of anisotropy effects onto the line profile. Hence the shape of all lines is similar, but the width at 193 nm is significantly broader than at 266 and 248 nm.

While the integrated line intensities are utilized to determine quantum yields, the width of a line profile is utilized to characterize the recoil velocity of the H/D products. Fig. 1 shows three H atom Doppler profiles resulting from HN_3 photolysis at three different excitation wavelengths. The width of the line profiles is nearly the same at an excitation wavelength of 266 and 248 nm, whereas a clearly broader profile is measured at 193 nm. A growth of the Doppler width with increasing available energy is not unexpected, but then it should also be observed when the photolysis wavelength is changed from 266 to 248 nm.

Fig. 2 shows two Doppler profiles detected in the photolysis of HN_3 at 248 nm using a linearly polarized photolysis laser. When the electric field vector of the photolysis light $\boldsymbol{E}_d$ is aligned parallel to the propagation direction of the probe laser $\boldsymbol{k}_a$ (geometry V), a rounded lineshape is detected (left side of Fig. 2). Switching to a perpendicular alignment between $\boldsymbol{E}_d$ and $\boldsymbol{k}_a$ (geometry II) results in a pro-

Table 1
Quantum yield ($\pm\sigma$) of the H/D + N_3 channel and absorption cross section data at 266, 248 and 193 nm

λ_p (nm)	$\phi_{H+N_3}(\lambda)$	$\sigma_{HN_3}(\lambda)$	$\sigma_{H_2S}(\lambda)$	$\phi_{D+N_3}(\lambda)$	$\sigma_{DN_3}(\lambda)$	$\sigma_{D_2S}(\lambda)$
266	4.2 ± 0.9	9.0×10^{-20}	$\sim 4.6 \times 10^{-22}$			
248	20 ± 4	6.5×10^{-20}	2.8×10^{-20}	17 ± 4	6.6×10^{-20}	6.4×10^{-21}
193	14 ± 2	2.0×10^{-18}	5.3×10^{-18}	14 ± 3	2.0×10^{-18}	6.8×10^{-18}

Units are % and cm^2/molec, respectively. Since σ_{H_2S}(266 nm) is extremely small, the fragmentation of HI is used as a reference system at this wavelength ($\sigma_{HI}(266\text{ nm}) = 1.8 \times 10^{-19}$ cm^2/molec [50]).

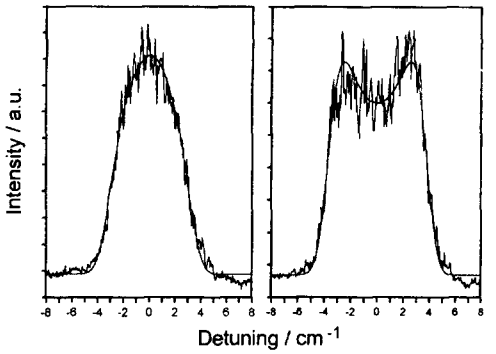

Fig. 2. H atom Doppler profiles from the fragmentation of HN_3 with polarized 248 nm radiation. When E_d is rotated from being parallel with respect to k_a (left side) to a perpendicular alignment (right side), a characteristic change of the lineshape is observed indicating $v_H \perp \mu_{HN_3}$. The solid line represents the outcome of the quantitative analysis.

nounced dip in the center of the Doppler profile (right side of Fig. 2). Consequently, the photofragments are ejected preferentially perpendicular to the electric field vector of the photolysis light. Since the probability for absorbing a photon goes as $P_{abs} = |E_d \cdot \mu_{HN_3}|^2$, a preferential ejection of the fragments perpendicular to E_d suggests that the electronic transition moment of HN_3 is perpendicular to the recoil axis connecting the H atom with the center-of-mass of the N_3 unit. For the photolysis of HN_3 at 266 nm and of DN_3 at 248 nm we find similar results.

The line profiles detected in the HN_3/DN_3 fragmentation at a photolysis wavelength of 193 nm, by

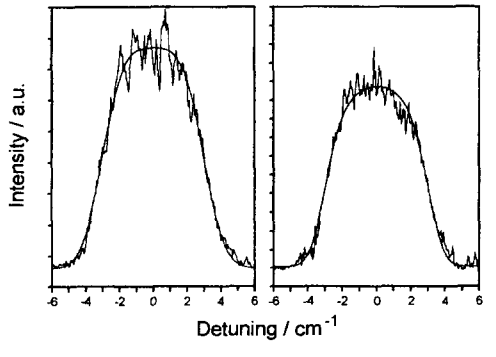

Fig. 3. D atom Doppler profiles resulting from the DN_3 photolysis at 193 nm. Changing the polarization geometry from $E_d \| k_a$ (left side) to $E_d \perp k_a$ (right side) has almost no influence on the lineshape. The solid line represents the outcome of the quantitative analysis.

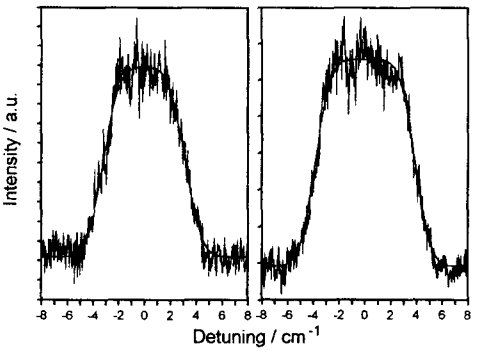

Fig. 4. H atom Doppler profiles from the 222 nm dissociation of HN_3. Changing the polarization geometry from $E_d \| k_a$ (left side) to $E_d \perp k_a$ (right side) has no influence on the lineshape, but the width varies.

contrast, are independent of the polarization geometry applied (see Fig. 3). For both the parallel and perpendicular alignment of E_d and k_a, the shape of the line profile is rather flat indicating that there is no preferred recoil direction. A surprising effect is observed in the 222 nm photolysis of HN_3. As in the HN_3/DN_3 photodissociation at 193 nm, the shape of the H atom Doppler profiles is not a function of the alignment between E_d and k_a, but the linewidth increases when the polarization geometry is varied from V to II (see Fig. 4). Using an unpolarized photolysis laser the linewidth lies between the limits of the polarization measurement.

Fig. 5 shows a Doppler profile detected in the DN_3 fragmentation using only the VUV probe laser. In difference to the measurements presented above where the signal generated solely by the VUV laser

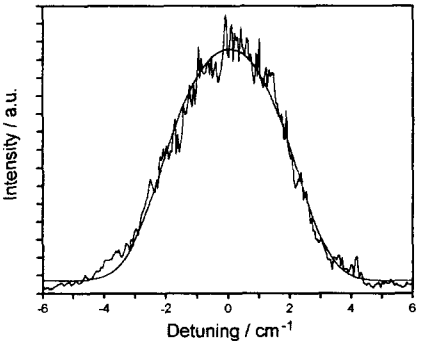

Fig. 5. D atoms from the photolysis of DN_3 at 122 nm. Since only the VUV probe laser is employed, only one polarization geometry is observable.

is minimized, in this experiment it is optimized. Compared to the line profile measured at 193 nm, the linewidth decreases although there is much more excess energy available. Also the shape of the profile is different. We note that the observed LIF signal depends strongly on the intensity of the 364.8 nm dye laser fundamental. A quantitative analysis reveals that the detected signal is induced by six photons of 364.8 nm wavelength which may be rationalized most probably by pump and probe in the VUV at 121.6 nm.

In order to extract quantitative results for the translational energy release and the vector correlation, we fit the functional form given below to the observed Doppler profiles:

$$D(\nu_a) = A\int_{\nu_0-\Delta\nu_D}^{\nu_0+\Delta\nu_D}[1+\beta P_2(\cos\theta)P_2(x_D)] \times G(\nu,\nu_a)\,d\nu + B, \quad (1a)$$

with

$$G(\nu,\nu_a) = \exp\left[-4\ln 2\left(\frac{\nu-\nu_a}{\Delta\nu_a}\right)^2\right] \quad (1b)$$

and

$$x_D = \frac{\nu-\nu_0}{\Delta\nu_D}. \quad (1c)$$

In the above equation β is the anisotropy parameter, $P_2(\cos\theta)$ and $P_2(x_D)$ are second-order Legendre polynomials, θ is the angle between the electric field of the photolysis laser and the propagation direction of the probe laser, x_D is the ratio of the displacement from line center $\nu-\nu_0$ to the maximum Doppler shift $\Delta\nu_D = \nu_0 v/c$, ν_a is the frequency of the probe laser and $\Delta\nu_a$ the effective width of the Gaussian convolution function $G(\nu,\nu_a)$. The parameters A and B allow us to scale the amplitude and baseline of the peaks.

The Gaussian convolution function accounts for the spectral broadening introduced by the finite linewidth of the probe laser ($\Delta\nu_{VUV} = 1.25$ cm^{-1}) and the wide recoil velocity distribution of the H atoms. Since the velocity of the ejected H atoms is extremely high compared to that of the HN_3 parent molecules, broadening induced by the thermal motion of the HN_3 molecules (0.16 cm^{-1}) is neglected. For the dissociation of HN_3/DN_3 it is known from the REMPI/TOF measurements that the H/D atom velocity distribution can be approximated by a Gaussian function centered around a mean velocity $\langle v\rangle$ [23]. In this case a least-squares fit of Eq. (1) to the detected H/D atom Doppler profiles reveals the anisotropy parameter β, the Doppler shift $\Delta\nu_D$ [1], and the effective width of the convolution function $\Delta\nu_a$. Through $\Delta\nu_f = (\Delta\nu_a^2 - \Delta\nu_{VUV}^2)^{1/2}$ and $\Delta v_f = c\Delta\nu_f/\nu_0$ we obtain the width of the Gaussian recoil velocity distribution.

While the above analysis proceeds via a forward calculation assuming a Gaussian recoil velocity distribution, other techniques exist which are based on Kinsey's Fourier transform inversion procedure in order to directly extract the recoil velocity distribution $f(v)$ [35–44]. Unfortunately, all these inversion procedures are very sensitive to noise in the data and the poor signal-to-noise ratio of our VUV Doppler profiles does not allow us to apply such a subtle technique.

All quantities gained by the forward calculation are summarized in Table 2. $\Delta\nu_D$, $\Delta\nu_f$, and β are given as the average of 6 to 10 measurements and the standard deviation is indicated. The error range of the anisotropy parameter measured in the VUV

Table 2
Quantitative results ($\pm\sigma$) from the analysis of the H/D atom Doppler profiles detected in the photolysis of HN_3/DN_3 at 266, 248, 222, 193 and 122 nm

	λ_p (nm)	$\Delta\nu_D$ (cm^{-1})	$\Delta\nu_f$ (cm^{-1})	β
HN_3	266	3.12±0.08	0.89±0.13	−0.56±0.14
	248	3.34±0.08	0.90±0.13	−0.72±0.16
	222V	3.39±0.22	1.83±0.18	−0.16±0.38
	222II	3.81±0.10	1.75±0.21	−0.06±0.26
	193	4.12±0.14	2.48±0.31	+0.08±0.16
	122	3.80±0.13	2.36±0.06	(+0.8)
DN_3	248	2.25±0.04	0.73±0.04	−0.60±0.14
	193	2.86±0.33	1.07±0.16	+0.04±0.30
	122	2.69±0.05	1.42±0.23	(+0.8)

A β parameter of -1 indicates a perpendicular alignment of the electronic transition moment and the recoil velocity vector; $\beta = 2$ indicates $\mu \| v$.

[1] Due to the splitting of the upper ^{2}P level an H atom Doppler profile consists of two lines separated by 0.365 cm^{-1}. This splitting is considered when determing the Doppler shift. The Doppler shift is reduced by ~ 2%.

photolysis is higher because in this experiment the electric field of the photolysis light can not be rotated with respect to the probe laser axis. For the photolysis at 222 nm we distinguish between the two polarization geometries applied.

4. Discussion

In order to discuss the dissociation dynamics, in particular the $\langle \boldsymbol{\mu} \cdot \boldsymbol{v} \rangle$ correlation, it is important to know the molecular structure of HN_3 which is shown in Fig. 6. The ground $\tilde{X}\,^1A'$ state has a planar equilibrium geometry consisting of an almost linear N_3 chain ($\alpha_{NNN} = 171.3°$) and a strongly bent NH bond ($\alpha_{NNH} = 108.8°$). Fig. 6 also illustrates the positions of the electronic transition moments for excitation of the first three excited singlet states that have been calculated by Meier and Staemmler [28–30]. While $\boldsymbol{\mu}(\tilde{A} \leftarrow \tilde{X})$ and $\boldsymbol{\mu}(\tilde{C} \leftarrow \tilde{X})$ are perpendicular to the plane of symmetry, $\boldsymbol{\mu}(\tilde{B} \leftarrow \tilde{X})$ lies in this plane enclosing an angle of 114° with the recoil coordinate $\boldsymbol{R}$.

The ab initio calculations indicate that several electronic states of HN_3/DN_3 might be accessed in the energy range corresponding to the photolysis wavelengths used in the present investigation: 266–122 nm. Likewise, the absorption spectrum shows features which can be related to the excitation of various electronic states [26,27]. Our data strongly support this expectation.

The H atom Doppler shifts measured in the photolysis of HN_3/DN_3 at 266 and 248 nm are comparable, whereas the line profile obtained in the 193 nm experiment is significantly broader. In the VUV photolysis at 122 nm the Doppler shift decreases again.

The anisotropy parameter is strongly negative at 266 and 248 nm, but at 222 and 193 nm the β parameter is close to zero. In the VUV fragmentation a positive β parameter is observed.

Therefore, we distinguish between three cases: excitation in the first absorption band at 266 and 248 nm, photodissociation at 222 and 193 nm, and finally photolysis in the VUV at 122 nm.

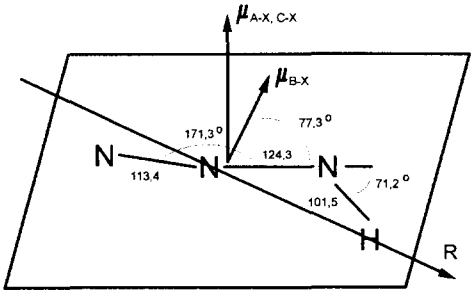

Fig. 6. Molecular structure of hydrazoic acid HN_3 in the ground $\tilde{X}\,^1A'$ state. Due to conservation of linear momentum the H and N_3 photofragments move along the recoil coordinate $\boldsymbol{R}$.

4.1. Dissociation in the first absorption band

In the case of a Gaussian-like recoil velocity distribution, the mean kinetic energy of the recoiling photofragments is given by

$$\langle E_{kin} \rangle = \frac{m_H^2}{2\mu} \langle v \rangle^2 \left[1 + \frac{1}{8 \ln 2} \left(\frac{\Delta v_f}{\langle v \rangle} \right)^2 \right]. \qquad (2)$$

In this equation μ represents the reduced mass of the $H–N_3$ system. Through conservation of energy one obtains the internal energy of the N_3 partner

$$\langle E_{int} \rangle = E_{av} - \langle E_{kin} \rangle, \qquad (3)$$

where $E_{av} = E_{h\nu} + E_{int}(HN_3) - E_{diss}$ is the available energy. The width of the internal energy distribution of the N_3 radical can be calculated from

$$\Delta E_{int} = \frac{m_H^2}{\mu} \langle v \rangle \Delta v. \qquad (4)$$

The energy disposal is summarized in Table 3. For $E_{diss}(H–N_3)$ we employ a value of 30870 cm^{-1} [23]. From this value $E_{diss}(D–N_3)$ is determined to be 31620 cm^{-1} by considering the difference between the zero-point energies of HN_3 and DN_3 vibrations [14]. In the photolysis of HN_3 at 266 nm much of the energy deposited in the parent molecule appears as product translation ($f_{kin} = 0.82$). An increase of the available energy causes only a slightly higher translation, whereas the internal energy of the N_3 partner fragment increases significantly. At 248 nm the internal energy of N_3 is found to be 3150 cm^{-1}, compared to 1250 cm^{-1} at 266 nm. Thus the dissociation of HN_3/DN_3 in the first absorption band is an example for the strong-coupling-limit and the excited potential energy surface is expected to

have strong gradients in other coordinates than the H/D–N_3 distance.

More information on the upper potential energy surface (PES) is extracted from the $\langle \boldsymbol{\mu} \cdot \boldsymbol{v} \rangle$ correlation measurement. The β parameter resulting from the dissociation of HN_3/DN_3 in the first absorption band is strongly negative indicating a preference for a perpendicular alignment of the electronic transition moment and the recoil velocity vector. Assuming that the dissociation process takes place in the plane of the parent molecule and the electronic transition moment is aligned perpendicular to this plane of symmetry, our findings predict that the excited electronic state is of A″ character, since the ground electronic state has A′ symmetry. We note that, in principle, the transition moment could also lie in the plane of symmetry but still be directed perpendicular to the recoil coordinate leading us to the conclusion that the excited electronic state is of A′ symmetry. However, the latter scenario is not in line with the ab initio calculations.

The calculations of Meier and Staemmler show an antisymmetric state at energies corresponding to the first absorption band. It is the first excited singlet state, labeled $\tilde{A}\,^1A''$. Furthermore the ab initio calculations demonstrate that an increase of the H–N_3 distance of the $\tilde{A}\,^1A''$ PES directly leads to $H(^2S)$ and $N_3(X\,^2\Pi_g)$ products. No level crossing or predissociation is necessary to explain the formation of the hydrogen product, but a barrier of at least 2300 cm^{-1} is calculated for the H–N_3 separation coordinate (see Fig. 7). Increasing the N_2–NH distance leads to $NH(a\,^1\Delta)$ and $N_2(X\,^1\Sigma^+)$ products showing a barrier of comparable height like the one in the H + N_3 channel [30].

In the following discussion we consider a mechanism on how the excited complex overcomes the barrier. Dealing with such details of the upper ab initio PES seems to over-stress the model. However, the agreement of theoretical and experimental results is excellent for the NH + N_2 channel [13,30]. This is supported not only by the concordance of the vertical excitation energy with the maximum of absorption, but also by the concordance of the calculated and measured oscillator strength of the first absorption band [26,30].

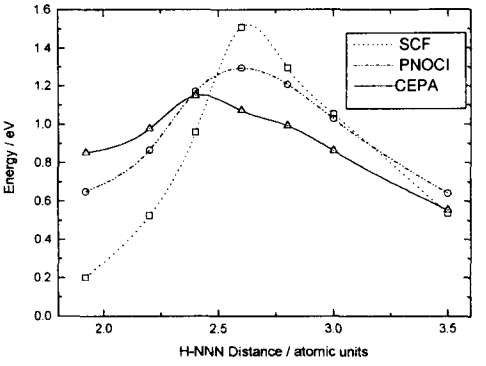

Fig. 7. Potential energy curves of $HN_3(\tilde{A}\,^1A'')$ along the H–N_3 coordinate. The potential energy is given relatively to the H and N_3 products. The curves are calculated by different methods: CEPA, PNOCI, and SCF. Even the most accurate CEPA calculation yields a significant barrier. The figure is adapted from Ref. [29].

In principle, the HN_3 molecule might dissociate by tunneling of the H atom through the barrier. The probability of tunneling through the barrier is calculated using the approximation of a rectangular barrier with a height of 2300 cm^{-1} and a width of 30 pm (the values are taken from Fig. 7) [45]. At a photolysis wavelength of 248 nm we obtain a probability of 57%. Due to the isotopic shift and the higher mass in

Table 3
Energetics resulting from the HN_3/DN_3 dissociation in the first absorption band

λ_p	R	E_{av}	$\langle v \rangle$	$\langle E_{kin} \rangle$	$\langle E_{int} \rangle$	ΔE_{int}	f_{kin}	f_{int}
266	H	7070	11370	5820	1250	3170	0.82	0.18
248	D	9090	8200	6350	2740	3860	0.70	0.30
248	H	9790	12170	6640	3150	3450	0.68	0.32
243	H	10340		6650	3690	3690	0.64	0.36

Units are m/s and cm^{-1}, respectively.
We emphasize the excellent agreement between the results of this work measured by LIF (first three rows) and the results of Ref. [23] measured by REMPI/TOF (last row).

the case of DN_3, the tunneling probability is reduced to 10%. However, the quantum yields of the H–N_3 and D–N_3 channel measured at 248 nm are equal within the experimental error and a contribution from tunneling should be small.

Another possibility to pass the barrier is internal energy redistribution (IVR). This mechanism requires some time, at least some picoseconds. The observed anisotropy parameter ($\beta_{HN_3}(248\ nm) = -0.72$ and $\beta_{DN_3}(248\ nm) = -0.60$), however, points to a direct fragmentation process occurring on the femtosecond time scale. If the excited parent molecule had a longer lifetime, its rotational motion would smear out any pronounced vector correlation. Following the work of Busch and Wilson [46], we estimate an upper limit of the dissociation time: $\tau_{HN_3} \leq 17$ fs and $\tau_{DN_3} \leq 31$ fs. Based on this, we predict a rapid dissociation process which is also indicated by the non-statistical energy distribution. Since tunneling or IVR is not in line with our experimental findings, the generation of H/D atoms in the photolysis of HN_3/DN_3 harmonizes only with the ab initio calculations if we assume that the excited complex bypasses the potential hill of the $\tilde{A}\,^1A''$ PES.

In the ab initio calculations only the N–H distance is varied, while the other variables are fixed to their equilibrium values of the ground $\tilde{X}\,^1A'$ state. The influence of the barrier will be reduced drastically if "vibrational motion" of HN_3/DN_3 changes this transition state geometry [47], i.e. other coordinates than the H–N_3 separation distance are involved in the fragmentation process. We note that such a picture is consistent with a dissociation in the strong-coupling-limit.

These findings might be compared with the $HN_3 \rightarrow N_2 + NH(^1\Delta)$ dissociation channel because there is also a barrier in the N_2–NH coordinate of the first excited $\tilde{A}\,^1A''$ state which is lowered by a N–N–N in-plane or out-of-plane motion (similar to the $\nu_5(a')$ and $\nu_6(a'')$ mode of hydrazoic acid). This motion dominates the whole dissociation process and as a consequence the N_2 product rotates strongly [1]. If the available energy is enhanced by using shorter photolysis wavelengths, the N_2 fragment picks up all additional energy, while the $NH(^1\Delta)$ molecule behaves like a spectator having the same kinetic and rotational energy [13]. Its vibrational energy, however, is not constant [15]. Since the same coordinate of the upper PES is responsible for NH vibration and H atom generation, we compare the results of Ref. [15] with ours.

Hawley et al. determined the vibrational state distribution of the NH fragments in dependence on the available energy using a tunable photolysis laser. As a result, the threshold wavelengths for forming NH in $v = 1$ and $v = 2$ were obtained: $\lambda(v = 1) = 282$ nm and $\lambda(v = 2) = 269$ nm. These values lie significantly above the thermodynamic thresholds of 476 and 417 nm. After reaching these wavelengths, the generation of vibrationally excited fragments increases much more than expected for a statistical process [15]. In the present work, we determine the quantum yield of the H + N_3 channel at 248 nm to be 20%, while it is only 4% at 266 nm. So the H + N_3 dissociation channel should be open somewhat below 266 nm which is clearly above the thermodynamical threshold of 324 nm. At a slightly shorter photolysis wavelength (248 nm) the contribution of the H atom channel increases significantly.

4.2. Photolysis at 222 and 193 nm

We use the same equations as above to calculate the energy disposal at a photolysis wavelength of 193 nm (see Table 4). In analogy to the dissociation in the first absorption band, mainly the N_3 radical picks up additional excess energy. But the trend is

Table 4
Energetics in the photolysis of HN_3/DN_3 at 193 nm

λ_p	R	E_{av}	$\langle v \rangle$	$\langle E_{kin} \rangle$	$\langle E_{int} \rangle$	ΔE_{int}	f_{kin}	f_{int}
193	D	20500	10420	10300	10200	7150	0.50	0.50
193	H	21240	15020	11640	9600	11700	0.55	0.45

Units are m/s and cm^{-1}, respectively.
As outlined below, the calculation of average kinetic energy releases is not justified at an excitation wavelength of 222 nm.

less pronounced. In the photolysis of HN_3 at 193 nm the kinetic energy of the products is calculated to be 11640 cm^{-1} and the internal energy of N_3 is 9600 cm^{-1}. The distribution of the internal energy is extremely broad: $\Delta E_{int} = 11640\ cm^{-1}$. These values differ from a statistical energy disposal and a rather direct dissociation is expected. This is supported by the equal quantum yields of the $H-N_3$ and $D-N_3$ channel and the smooth and unstructured absorption spectrum around 193 nm [26].

For this reason one might expect a pronounced $\langle \boldsymbol{\mu} \cdot \boldsymbol{v} \rangle$ correlation. In the photolysis of HN_3 at 193 nm, however, the spatial distribution of the fragments is characterized by a β parameter which is close to zero. This may have various reasons: (a) a pronounced vector correlation is smeared out by rotation of a long-living excited complex, (b) the angle between $\boldsymbol{\mu}_{HN_3}$ and $\boldsymbol{v}_H$ is 54.7° (magic angle), or (c) different electronic states are involved in the dissociation process similar to the photolysis of H_2O_2 at 193 nm [48]. Due to the non-statistical energy distribution the first case is not very likely. As (b) is concerned, we cannot completely rule it out. But from the calculations it is known that for a fragmentation out of the ground state geometry the angle between the electronic transition moment and the recoil velocity vector differs significantly from 54.7° as illustrated in Fig. 6.

This leads us to the conclusion that more than one excited electronic state is involved in the photolysis of HN_3 at 193 nm. This notion is consistent with several other findings. First, the absorption spectrum of HN_3 shows a "shoulder" around 200 nm which may be caused by two almost entirely overlapping bands. The ab initio calculations of Meier and Staemmler yield two excited singlet states, $\tilde{B}\,^1A'$ and $\tilde{C}\,^1A''$, in the energy region corresponding to 200 nm [28]. Furthermore the HN_3 photolysis at 193 nm gives rise to NH products in all energetically accessible electronic states: $X\,^1\Sigma^-$, $A\,^1\Pi$, $a\,^1\Delta$, $b\,^1\Sigma^+$, and $c\,^1\Pi$ [2]. Since the $\tilde{B}\,^1A'$ state of HN_3 correlates with $NH(b\,^1\Sigma^+)$ and the $\tilde{C}\,^1A''$ state correlates with $NH(c\,^1\Pi)$, the excitation of both electronic states of HN_3 is plausible [30].

For a fragmentation out of the ground state geometry the angle between $\boldsymbol{\mu}(\tilde{B}\,^1A' \leftarrow \tilde{X}\,^1A')$ and $\boldsymbol{v}$ is about 114°, while $\boldsymbol{\mu}(\tilde{C}\,^1A'' \leftarrow \tilde{X}\,^1A')$ and $\boldsymbol{v}$ are aligned perpendicular to each other. Applying $\beta = 2\beta_{\mu v} = 3\cos^2\theta_{\mu v} - 1$, we estimate the theoretical β parameters for a pure excitation of either the $\tilde{B}$ or the $\tilde{C}$ state: $\beta(\tilde{B} \leftarrow \tilde{X}) = 0.44$ and $\beta(\tilde{C} \leftarrow \tilde{X}) = -1$. Following the work of Grunewald et al. [48] we write

$$\beta_{obs} = b\beta(\tilde{B} \leftarrow \tilde{X}) + c\beta(\tilde{C} \leftarrow \tilde{X}) \text{ with } b + c = 1$$

for the simultaneous excitation of both states where b and c are the relative contributions of the $\tilde{B}$ and $\tilde{C}$ state (quantum mechanical interferences [49] are neglected). It should be mentioned that b and c are not the H atom quantum yield ϕ_B or ϕ_C, but the product of the differential cross section σ_B and ϕ_B (or $\sigma_C \cdot \phi_C$). In the photolysis of HN_3 at 193 nm, we find $\beta_{obs} \approx 0$ and the relative contributions b and c are estimated at $b \approx 0.70$ and $c \approx 0.30$. The same values are obtained for the 193 nm photodissociation of DN_3.

To check the assumption that two excited states are accessed, the photolysis wavelength is changed to 222 nm. Since this wavelength is at the long-wavelength limit of the second absorption band, the lower-lying $\tilde{B}\,^1A'$ state should contribute more to the H atom generation. Therefore we expect a preference for a positive anisotropy parameter. The β parameter measured at 222 nm, however, is close to zero as that determined in the photolysis at 193 nm. On the other hand, the width of the line profile is a function of the polarization geometry in the 222 nm experiment. For a parallel alignment of $\boldsymbol{E}_d$ and $\boldsymbol{k}_a$ the Doppler shift is $3.39 \pm 0.2\ cm^{-1}$ and for $\boldsymbol{E}_d \perp \boldsymbol{k}_a$ this value increases to $\Delta\nu_D = 3.81 \pm 0.1\ cm^{-1}$.

In the following discussion we present a possible explanation for this phenomenon which is also based on the assumption of access to two excited states. As mentioned above, the electronic transition moment for exciting the $\tilde{B}\,^1A'$ state, $\boldsymbol{\mu}(\tilde{B} \leftarrow \tilde{X})$, lies in the plane of symmetry, while $\boldsymbol{\mu}(\tilde{C} \leftarrow \tilde{X})$ is perpendicular to it. For a parallel alignment of $\boldsymbol{E}_d$ and $\boldsymbol{k}_a$ the exclusive excitation of the $\tilde{B}$ state leads to a profile with a dip in the center of the line, while fragmentation from the $\tilde{C}$ state results in a rounded Doppler profile. For a perpendicular alignment of $\boldsymbol{E}_d$ and $\boldsymbol{k}_a$ one obtains a rounded profile for a dissociation from the $\tilde{B}$ state and a dipped line when the $\tilde{C}$ state is excited exclusively.

If both states contribute to the H atom generation, the observed line profile will be a superposition of a

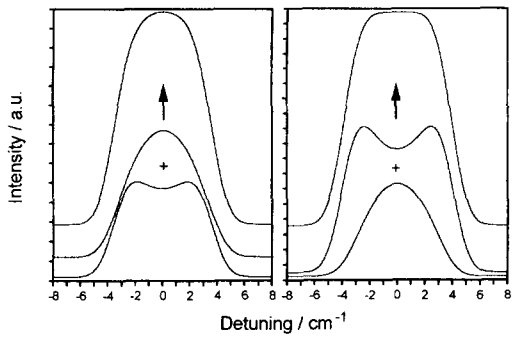

Fig. 8. For a superposition of a dipped and a rounded profile having moderately different Doppler shifts, the dipped contribution determines the width of the composite line profile.

dipped and a rounded line profile (see Fig. 8). It is likely that different repulsive states generate H atoms with different velocities, i.e. different linewidths are expected. But then the average width of the composite line in both polarization geometries is dominantly determined by the contribution of the dipped profile. In other words, the anisotropy parameter becomes velocity dependent.

For an illustration of this effect Fig. 8 shows the superposition of two lines having individual Doppler shifts of 3.39 and 3.81 cm^{-1}. $\boldsymbol{E}_p \perp \boldsymbol{k}_a$ results in a superposition of a dipped line profile (from faster H fragments which correlate with $\tilde{C}\,^1A''$) with a rounded profile (from slower H fragments which correlate with $\tilde{B}\,^1A'$) as one can see on the right side of Fig. 8. In this polarization geometry a Doppler shift of 3.79 cm^{-1} is obtained if a single line form function is fitted to the composite line. Thus the width of the composite line is caused by the broad dipped contribution. In the other geometry, by contrast, a broad rounded profile is added to a narrow dipped one (left side of Fig. 8). A fit to the resulting line profile yields a Doppler shift of 3.48 cm^{-1}. Again the width of the observed Doppler profile is determined by the dipped contribution and, therefore, it is narrower. At a photolysis wavelength of 193 nm this effect is not noticeable and the average over both geometries is taken as usual.

4.3. Fragmentation at the probe laser wavelength (122 nm)

At a photolysis wavelength of 122 nm the H atoms can be generated according to different dissociation channels which are summarized in Table 5. The first fragmentation channel, which leads to H + N_2 + N(^{4}S), is less likely because the conservation of spin is violated. For channel 2 leading to H + $N_3(\tilde{X})$, an extremely high excess energy is released resulting in fast H/D atoms, i.e. in a broad Doppler profile. However, a fairly narrow line is observed in the experiment. From the Doppler shift the average kinetic energy is determined to be only 10000 cm^{-1} in the VUV photolysis of HN_3 and 9750 cm^{-1} in the VUV photolysis of DN_3. Consequently, the formation of N_3 in the ground electronic state seems to be unlikely.

A three-body decay as described by channel 3 and 4 of Table 5 does not restrict the recoil velocity like in the case of a two-body decay. However, we can calculate the highest possible H atom velocity. For the formation of H + N_2 + N(^{2}D), a maximum kinetic energy of $E_{kin,max}$ = 32200 cm^{-1} is obtained. If the H atoms are generated via channel 4 giving H + N_2 + N(^{2}P), $E_{kin,max}$ is reduced to 22800 cm^{-1}. Experimentally, the maximum kinetic energy is extracted from the base of an H/D atom Doppler profile. We obtain a maximum kinetic energy of $E_{kin,max}$(H) = 14600 cm^{-1} for the dissociation of HN_3 and $E_{kin,max}$(D) = 11100 cm^{-1} for the dissociation of DN_3. Although an extrapolation to the largest Doppler broadening is associated with a lower accuracy than the determination of the Doppler shift, the experimentally obtained maximum kinetic energies are significantly smaller than those calculated for the three-body decays 3 and 4.

Another possibility is the sequential decay $HN_3 \rightarrow N_2 + NH \rightarrow N_2 + N + H$ which also leads to the products of channel 3 and 4. We distinguish between two limiting scenarios. In the first scenario the NH

Table 5
Energetically allowed fragmentation channels that generate H atoms in the photolysis of HN_3 at 122 nm; channel 1 is spin-forbidden

Products	E_{diss} (cm^{-1})	λ_p (nm)	Determination of E_{diss}	
H + N_2 + N(^{4}S)*	30470	328.2	channel 2 Ref. [51]	(1)
H + $N_3(\tilde{X}\,^2\Pi)$	30870	323.9	measured [23]	(2)
H + N_2 + N(^{2}D)	49670	201.3	1 + T_e(N) [51]	(3)
H + N_2 + N(^{2}P)	59270	168.7	1 + T_e(N) [51]	(4)
H + $N_3(\tilde{A}\,^2\Sigma)$	67170	148.9	2 + $T_e(N_3)$ [25]	(5)

intermediate receives an amount of energy which is just sufficient to break the NH bond. In this case the recoil velocity of the H atom might be very small. The other extreme of a sequential decay involves a dissociation into N_2 and NH where the NH intermediate is strongly excited. In the second step much of this energy is released as H atom translation. We calculate a maximum kinetic energy of 21800 cm^{-1} for channel 4 and 30800 cm^{-1} for channel 3. The experimental value lies between the limits of the two scenarios and a sequential decay cannot be ruled out by this analysis. The positive anisotropy parameter, however, implicates a direct fragmentation process without relaxation of the anisotropic H atom recoil velocity distribution induced by the rotational motion of a long-living NH intermediate.

Thus we favor the last dissociation channel given in Table 5 which leads to $H + N_3(\tilde{A}\,^2\Sigma)$ where the N_3 fragment is generated in the first excited electronic state. The maximum kinetic energy for the H atoms generated via channel 5 is 15100 cm^{-1} which is in very good agreement with the experimental value of 14600 cm^{-1}. We use the measured Doppler shift along with the dissociation energy which is necessary for the generation of $H/D + N_3(\tilde{A})$ fragments to calculate the average internal energy of the $N_3(\tilde{A})$ partner. One obtains 5470 cm^{-1} for N_3 resulting from the 122 nm photolysis of HN_3 and 4980 cm^{-1} for N_3 resulting from the 122 nm photolysis of DN_3.

5. Conclusions

Polarization/Doppler spectroscopy has been used frequently to characterize diatomic photofragments. In the present study we apply this technique to analyze H and D atoms generated in the photolysis of HN_3 and DN_3 at different excitation wavelengths: 266, 248, 222, 193 and 122 nm. The measurements reveal the quantum yield of the $H–N_3$ and $D–N_3$ channel, the kinetic energy of the photofragments, and their spatial distribution.

The results indicate that at a photolysis wavelength of 266 and 248 nm only the first excited singlet state of HN_3/DN_3, $\tilde{A}\,^1A''$, is accessed on which a rapid dissociation process takes place. Excitation at a wavelength of 222 and 193 nm leads to a complex fragmentation via the $\tilde{B}\,^1A'$ and $\tilde{C}\,^1A''$ state. In the VUV photolysis at 122 nm the access to a higher-lying state is gained resulting in the formation of H/D atoms and electronically excited $N_3(\tilde{A})$ radicals.

Acknowledgements

This work has been supported by the Deutsche Forschungsgemeinschaft. Useful discussions with V. Staemmler and U. Meier are gratefully acknowledged.

References

[1] J.-J. Chu, P. Marcus and P.J. Dagdigian, J. Chem. Phys. 93 (1990) 257.
[2] F. Rohrer and F. Stuhl, J. Chem. Phys. 88 (1988) 4788.
[3] J.C. Stephenson, M.P. Casassa and D.S. King, J. Chem. Phys. 89 (1988) 1378.
[4] B.R. Foy, M.P. Casassa, J.C. Stephenson and D.S. King, J. Chem. Phys. 89 (1988) 608.
[5] B.R. Foy, M.P. Casassa, J.C. Stephenson and D.S. King, J. Chem. Phys. 90 (1989) 7037.
[6] M.P. Casassa, B.R. Foy, J.C. Stephenson and D.S. King, J. Chem. Phys. 94 (1991) 250.
[7] J.R. McDonald, R.G. Miller and A.P. Baronavski, Chem. Phys. Letters 51 (1977) 57.
[8] B.M. Dekoven and A.P. Baronavski, Chem. Phys. Letters 86 (1982) 392.
[9] A.P. Baronavski, R.G. Miller and J.R. McDonald, Chem. Phys. 30 (1978) 119.
[10] K.-H. Gericke and R. Theinl, J. Chem. Soc. Faraday Trans. 2 (1989) 85.
[11] K.-H. Gericke, R. Theinl and F.J. Comes, J. Chem. Phys. 92 (1990) 6548.
[12] H.H. Nelson and J.R. McDonald, J. Chem. Phys. 93 (1990) 8777.
[13] K.-H. Gericke, T. Haas, M. Lock, R. Theinl and F.J. Comes, J. Phys. Chem. 95 (1991) 6104.
[14] K.-H. Gericke, M. Lock, R. Fasold and F.J. Comes, J. Chem. Phys. 96 (1992) 422.
[15] M. Hawley, A.P. Baronawski and H.H. Nelson, J. Chem. Phys. 99 (1993) 2638.
[16] T. Hikida, Y. Maruyama, Y. Saito and Y. Mori, Chem. Phys. 121 (1988) 63.
[17] K.H. Welge, J. Chem. Phys. 45 (1966) 4373.
[18] B.A. Thrush, Proc. Roy. Soc. A 235 (1956) 143.
[19] R.S. Konar, S. Matsumoto and B. de B. Darwent, Trans. Faraday Soc. 67 (1971) 1698.
[20] D.E. Milligan and M.E. Jacox, J. Chem. Phys. 41 (1964) 2838.

[21] R.J. Paur and E.J. Bair, Intern. J. Chem. Kinet. 8 (1976) 139.
[22] K.-H. Gericke, M. Lock and F.J. Comes, Chem. Phys. Letters 186 (1991) 427.
[23] T. Haas, K.-H. Gericke, C. Maul and F.J. Comes, Chem. Phys. Letters 202 (1993) 108.
[24] G. Chambaud and P. Rosmus, J. Chem. Phys. 96 (1992) 77.
[25] A.E. Douglas and W. Jeremy Jones, Can. J. Phys. 43 (1965) 2216.
[26] J.R. McDonald, J.W. Rabalais and S.P. McGlynn, J. Chem. Phys. 52 (1970) 1332.
[27] H. Okabe, J. Chem. Phys. 49 (1968) 2726.
[28] U. Meier and V. Staemmler, Theoret. Chim. Acta 76 (1989) 95.
[29] U. Meier, Dissertation, Ruhr-Universität Bochum (1988).
[30] U. Meier and V. Staemmler, J. Phys. Chem. 95 (1991) 6111.
[31] G.C. Bjorklund, IEEE 11 (1975) 287.
[32] R. Mahon, T.J. McIlrath, V.P. Myerscough and D.W. Koopmann, IEEE 15 (1979) 444.
[33] D. Cotter, Opt. Commun. 31 (1979) 397.
[34] K.-H. Gericke, S. Klee, F.J. Comes and R.N. Dixon, J. Chem. Phys. 85 (1986) 4463.
[35] J.L. Kinsey, J. Chem. Phys. 66 (1977) 2560.
[36] N. Smith, T.A. Brunner and D.E. Pritchard, J. Chem. Phys. 74 (1981) 467.
[37] N. Smith, T.P. Scott and D.E. Pritchard, J. Chem. Phys. 81 (1984) 1229.
[38] J. Ticktin and R. Huber, Chem. Phys. Letters 156 (1989) 372.
[39] C.A. Taatjes, J.I. Cline and S.R. Leone, J. Chem. Phys. 93 (1990) 6554.
[40] F.J. Aoiz, M. Brouard, P.A. Enriquez and R. Sayos, J. Chem. Faraday Trans. 89 (1993) 1427.
[41] M. Brouard, S. Duxon, P.A. Enriquez and J.P. Simons J. Chem. Faraday Trans. 89 (1993) 1435.
[42] M. Brouard, H.M. Lambert, J. Short and J.P. Simons, J. Phys. Chem. 99 (1995) 13571.
[43] M. Dubs, U. Brühlmann and J.R. Huber, J. Chem. Phys. 84 (1986) 3106.
[44] M.P. Docker, Chem. Phys. 135 (1989) 405.
[45] A. Messiah, Quantum mechanics (North-Holland, Amsterdam, 1965).
[46] G.E. Busch and K.R. Wilson, J. Chem. Phys. 56 (1972) 3638.
[47] V. Staemmler, private communication.
[48] A.U. Grunewald, K.-H. Gericke and F.J. Comes, J. Chem. Phys. 87 (1987) 5709.
[49] I. Levy and M. Shapiro, J. Chem. Phys. 89 (1988) 2900.
[50] J.F. Ogilvie, Trans. Faraday Soc. 67 (1971) 2205.
[51] R.E. Continetti, D.R. Cyr, D.L. Osburn, D.J. Leahy and D.M. Neumark, J. Chem. Phys. 99 (1993) 2616.